



Batch adsorption of Fe^{3+} ions from aqueous solutions using activated carbon derived from Horse Chestnut Shells found in Northwestern Himalayas: Equilibrium, kinetic and thermodynamic studies

Uzma Imtiyaz¹ · Mushtaq Ahmad Rather¹

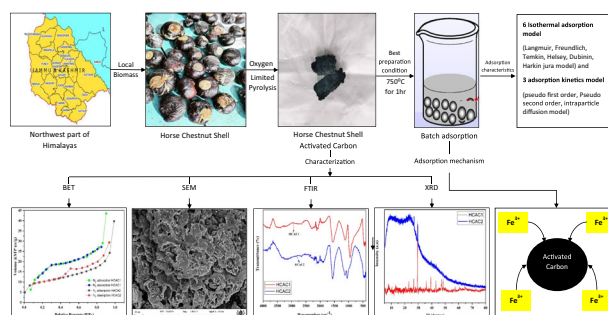
Received: 22 July 2024 / Accepted: 4 September 2024

© The Author(s), under exclusive licence to Springer Science+Business Media, LLC, part of Springer Nature 2024

Abstract

This research paper analyses the adsorbent properties of a unique biomass i.e. horse chestnut shell (*Aesculus hippocastanum L*) activated carbon synthesized by chemical activation of KOH produced under optimized carbonization conditions for Fe^{3+} . Research was done to look into the characteristics of the made activated carbon and its systematic effects of process parameters. Characterizations like SEM, BET, FTIR, XRD, TGA, EDX, proximate and ultimate analysis, calorific value was performed. Also effect of process parameters like initial Fe^{3+} ion content, contact time, dosage and temperature of system was studied for mechanism of adsorption at pH (6) of Fe^{3+} in an aqueous solution. Data on equilibrium and kinetic isotherms from experiments were examined, for kinetics pseudo 1st order reaction, pseudo 2nd order reaction and intraparticle diffusion has been utilised. System was fairly fitted by pseudo-2nd-order reaction. Adsorption isotherms such as Halsey, Harkin Jura, Temkin, Freundlich, and Langmuir and Dubinin Radushkevich were used and Langmuir adsorption isotherm turned out best suitable match as R^2 value was found out to be 0.99. The maximum Fe^{3+} adsorbing ability of the HCAC4 was 138.88 mg/g at 25 °C. Thermodynamical evaluation concluded the process to be spontaneous and heat-releasing.

Graphical Abstract



Keywords Activated carbon · Horse chestnut shell · Chemical activation · Adsorption · Wastewater

✉ Uzma Imtiyaz
uzma6phd19@nitsri.ac.in

¹ Department of Chemical Engineering, National Institute of Technology, Srinagar, India

Highlights

- Horse chestnut shell biomass was converted to activated carbon using KOH activation.
- Characterization (SEM, BET, FTIR, XRD, TGA, EDX) revealed favourable structural and compositional properties.
- Investigated effects of Fe³⁺ ion content, contact time, dosage, and temperature, achieving 138.88 mg/g adsorption at 25 °C.
- Pseudo-second-order kinetic model and Langmuir isotherm ($R^2 = 0.99$) best described the adsorption process.
- The process was spontaneous and exothermic, showing high potential for Fe³⁺ removal in water treatment.

1 Introduction

The environment's rising heavy metal concentrations present a serious risk to ecological systems, individual well-being, and other things. Of all the contaminants found within water, heavy metals have the greatest detrimental influence on the surroundings all over the globe [1, 2]. Big industries like leather, metallurgy, petroleum, batteries, textile, fertilizers, nuclear power, and pesticides are the origin of pollution caused by heavy metal [3]. Even at low concentrations, heavy metals are unfortunately incapable of being biodegraded, which causes them to accumulate inside living things and result in a variety of illnesses and problems [4].

A heavy metal which is commonly present in effluent water is iron, which poses risks to both the environment and people when it is present in excess. The recommended level of iron in drinking water as per WHO [5] and Indian standards ("[6] Indian Standard Drinking Water- Specification (Second Revision," n.d.) is 0.3 mg/L. It is generally found in groundwater, pickling waste, as well as from dispersed sources including combustion wastes, pipes, product ingredients, steel manufacturing plants, foundries, smelters, chemical mills, wire drawing processes, etc. [2]. Iron does not dissolve in water it instead forms ferric ions with a reddish-brown precipitate when it comes into contact with air [7]. It is impossible to remove or destroy the iron precipitates because of their stability and persistence in the environmental pollutants. Its concentration can be decreased.

There are different investigations and methods to remediate heavy metals such as Fe³⁺ from water these include leaching [8], adsorption, membrane filtration, solvent extraction, reduction, ion exchange, oxidation, and bioremediation, electrochemical treatment of all the above-named processes, adsorption has mainly been employed for treatment of heavy metals in aqueous system because of its easy process, scalability, low cost, originality [9].

Various adsorbent substances have been developed for a prolonged time interval and a lot of these substances have proven to be efficient in removing target pollutants and have been successful in extensive applications [10]. After using bio-adsorbents obtained from waste biomass, a lot of environmental problems and expense issues associated to

various treatments can be resolved. Activated carbons have been extensively made to use around the world for removing heavy metals and other water treatment methods.

Although they are available, commercial activated carbons are pricey. Therefore, in order to create inexpensive activated carbons, researchers are searching for appropriate natural raw materials. It should be mentioned that these raw materials need to be easily accessible and reasonably priced. Byproducts or residues from industry and agriculture are those raw materials that can be profitably transformed into activated carbon [11, 12]. Recently, a number of species, such as coconut shell [13], cashew nut shell [14], oil palm shell [15], hazelnut hull [16], kavath shell [17], rice husk ash [18], pecan shells [19], cactus fruit [20], pomegranate peels [21], sawdust of deciduous trees [22], almond shell [23], walnut shell olive stone [24] and many other agricultural wastes have been successfully converted into activated carbon and then brought to use perfectly.

In present study, the activated carbons are produced from horse chestnut shell present in the central part of north-western region of Himalayas scientifically named as *Aesculus hippocastanum* L. The horse chestnut shells exceptionally high carbon content (68.23%) revealed by proximate and ultimate analysis in this study underscores their potential to be novel and act as a promising source of raw material for preparation of activated carbon. The horse chestnut shell comes from the horse chestnut trees. These trees are distributed in the Himalayas from Kashmir to Nepal at an altitude of 900 to 3600 m. The shells are the outer coverings of the tree's nuts and are also known as conkers. In Kashmir (Northwestern Himalayas) these trees are used for beautification purposes, and these also have medicinal benefits when subjected to proper processing and purification. Horse chestnut shells are cost effective than other traditional raw materials like almond shells and coconut shells as they are free and readily available. In fact, when these horse chestnut shells are left unattended on the ground, they cause acidification of soil due to their low pH and thus harm the plants and micro-organisms. They take time in decomposition hence can tie up the soil nutrients like nitrogen, phosphorous making them unavailable for plants. Their presence on the ground can deplete the soil structure due to the presence of high lignin content. These also promote weed growth if not managed properly. It

therefore makes horse chestnut shells a better option to use as a raw material for development of useful substances in this case activated carbon and thereby stopping the above-mentioned disadvantages.

The development of effective adsorbents has become necessary because to the growing worries about heavy metal contamination, specifically iron (Fe^{3+}) ions. Activated carbon has been a popular choice because of its high surface area and porosity. The purpose of this work is to maximise Fe^{3+} adsorption capacity from aqueous solutions by synthesising and characterising activated carbon from horse chestnut shell (*Aesculus hippocastanum L*) utilising potassium hydroxide (KOH) as an activating agent. While KOH was chosen for its greater ability to build a highly porous structure that boosts adsorption capacity, horse chestnut shell was chosen for its abundance, affordability, and high carbon content. The use of KOH in this work enabled the production of a microporous structure that considerably enhanced the surface area and pore volume, hence enhancing Fe^{3+} adsorption efficiency. This is in contrast to prior studies that used activating agents such H_3PO_4 , ZnCl_2 , or steam. To produce activated carbon with improved adsorptive qualities and a larger yield, the carbonisation settings were also thoroughly adjusted. The number of methods, including N_2 adsorption/desorption, Fourier transform infrared spectroscopy (FTIR), scanning electron microscopy (SEM), and X-ray diffraction (XRD), were employed to analyse produced activated carbons. The process factors such as temperature, contact time, adsorbent dosage, and initial Fe^{3+} ion concentration were systematically investigated. This allowed for the fine-tuning of adsorption mechanisms, leading to greater performance than previously published research. The production of activated carbon with superior adsorption capabilities was made possible by the combined approach of choosing an ideal precursor, utilising KOH activation, and fine-tuning process parameters. This was demonstrated by the higher adsorption capacity and better fit to adsorption models in comparison to previous research.

2 Materials and methodology

2.1 Materials

Horse chestnuts were gathered from nearby trees in the Srinagar district of Kashmir, which is located in the central region of the Northwestern Himalayas. After the nuts were picked up and their shells removed, they were repeatedly cleaned using normal and deionized water to make them impurity less. Afterwards, the shells were oven dried for 24 h at 105 °C and kept in the sun for some days to dry. After the shells had dried completely, they were grounded into tiny fragments, milled, and screened. For the experiments, the fraction whose particle sizes fell between 0.80 and 1.00 mm was chosen.

2.2 Synthesis of activated carbon using KOH

KOH was utilised for the chemical activation of horse chestnut shells because of its proven ability to yield materials with a high surface area and well-developed pore structure, both of which are essential for improving adsorption capacity. KOH was selected as the activating agent for the synthesis of activated carbon. By interacting with carbon at high temperatures, the chemical activation procedure with KOH produces a controllable pore size distribution, resulting in a highly porous structure suitable for certain applications. KOH has a proven track record of effectiveness when compared to other activating agents and provides benefits for the environment and economy in the form of manageable byproducts and increased yields. The division of weights of KOH and utilized horse chestnut shells in the solution was used to get the impregnation ratio. The ratios of impregnation that were chosen were 1 and 3. After dissolving 20 g and 60 g KOH samples in distilled water (200 mL), dried horse chestnut shells weighing 20 g were combined with the KOH solution and agitated for six hours at about 80 °C. The KOH impregnated horse chestnut shells were put inside a ceramic boat, then carbonized in the tube furnace having 100 mL/min nitrogen flow rate at temperatures between 650 °C and 750 °C. The heat was provided to the samples from ambient temperature to the required temperature at a 10 °C/min rate to start the carbonization process. Samples were kept for sixty minutes at the ultimate temperature. To wash the resulting activated carbons, distilled water which was hot was used until the solution's pH was reached [25].

2.3 System boundary and flowchart

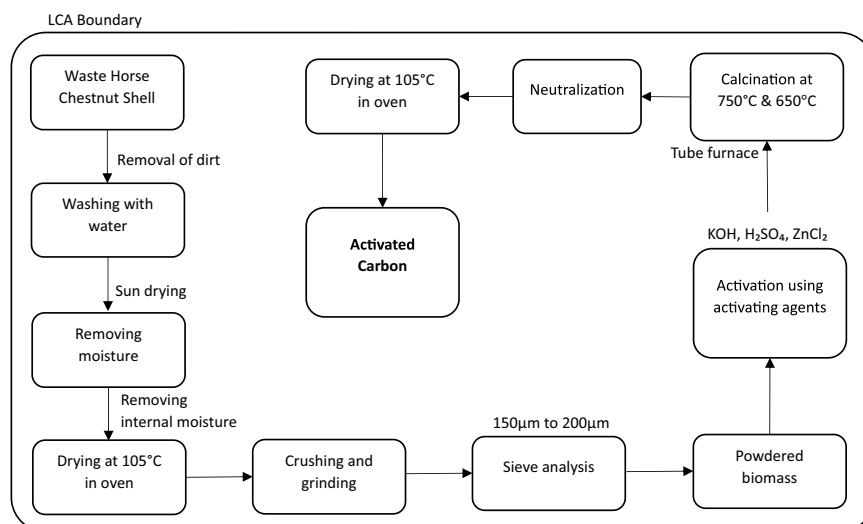
The term “system boundary” refers to a collection of specifications that specifies unit operations being a part of the product system, (ISO14040 2006a; b). There is an eleven-step process for producing activated carbon shown in Fig. 1. It starts with the collection of waste horse chestnuts, goes through washing the raw materials, removing moisture, drying the raw materials, crushing and grinding the materials, goes through a sieve, produces biomass powder, is impregnated with different activation agents, is calcinated, neutralized, and ends with drying the finished product. For every arrangement, the input and output are identified.

2.4 Characterization of raw material and activated carbon

2.4.1 Calorific value

The bomb calorimeter was used to calculate the horse chestnut sample's calorific value. When assessing the

Fig. 1 Eleven step Ac Production Process



energy content of fuels, including biomass like horse chestnut shells, the calorific value measured by bomb calorimetry is a crucial factor to consider. The first law of thermodynamics, which states that energy cannot be generated or destroyed, only altered, forms the basis of a bomb calorimeter's operation. Within a bomb calorimeter, combustion converts the chemical energy in a fuel into thermal energy, or heat. The amount of energy present in the fuel is then measured by measuring the temperature increase that occurs when this heat is transferred to a known volume of water.

2.4.2 Proximate and ultimate analysis

Using ASTM standard test procedures, the horse chestnut shell's proximate analysis (moisture content, ash content, and volatile matter) was computed. Amount of moisture was determined utilising a moisture analyser, and a muffle furnace was employed to determine the amount of ash and volatile matter. From there difference, fixed carbon was computed. A LECO-CHNS-932 elemental analyser was utilised to find the carbon, hydrogen, and nitrogen in elemental form from the horse chestnut shell. Table 1 presents the outcomes of the proximate and ultimate analysis of horse chestnut shell and the prepared activated carbon. Based on the results of proximate and ultimate analysis of the raw material (horse chestnut shell) it was confirmed that the presence of carbon in the precursor is abundant and can be processed further and converted into activated carbon.

2.4.3 Surface area analysis

Using the Quantachrome Nova Win2© 1994–2002 instrument and the BET (BHT) equation, surface area, volume of pores, and size distribution of pores of the prepared

Table 1 Proximate and ultimate analyses of Chestnut shell

Analysis	Characteristic	% Weight	ASTM test Standard
Proximate analysis	Moisture	9.67	D 2016–74
	Ash content	2.00	D 1102–84
	Volatile matter	60	E 897–82
	Fixed Carbon	28.33	-
Ultimate Analysis	Carbon	68.213	
	Hydrogen	8.906	
	Nitrogen	3.30	
	Sulphur	0.192	
	C/N ratio	20.670	
	C/H ratio	7.661	
	Empirical Formula	$C_{15}H_{16}O_9$	

activated carbons was ascertained using adsorption isotherms. A nitrogen molecule's cross-sectional area is kept 0.162 nm. To determine the micropore volume, the equation of Dubinin–Radushkevich (DR) was applied. Maintaining relative pressure of 0.985, the liquid volume of the adsorbate (N_2) was calculated to be the total pore volume. The BJH model was utilised to measure the distribution of pore size. The mean diameter of pore was measured by multiplying the total volume of pore by four across the BET surface area [26].

2.4.4 Scanning electron microscopy (SEM)

Horse chestnut shell was subjected to morphological analyses utilizing a scanning electron microscope (Leica Cambridge S-360). Carbon adhesive tabs which are double-sided electrically-conductive were used for placement of the samples onto the SEM holder so that the specimen's

surfaces wouldn't be exposed to the electron beam. A thick layer of gold approx. 20 nm was subsequently applied to the sample and was then operated in the SEM for 10 min using voltage 1.2 kV (10 mA) and a 20 Pa vacuum [26].

2.4.5 Fourier transform infrared analysis

An instrument Model 360 by Nicolet Avatar (FT-IR Spectrophotometer) that uses potassium bromide pellets at 4000 to 400 cm^{-1} wavelength was used. FTIR spectra was formed using dry powdered sample recorded on KBr disks of a Fourier Transform Infrared Spectrophotometer. Samples measuring 1 mg were mixed approximately in a potassium bromide matrix and formed pellets by pressing [27].

2.4.6 X-ray diffraction

XRD is the convenient method to evaluate size of nanoparticles, crystalline and amorphous substances. To ascertain the crystalline or amorphous nature of the activated carbon, X-ray diffraction analysis was completed. The Cu-K ($=0.15406 \text{ \AA}$) radiation source, running at 40 kV and 25 mA, was used for the analysis, which were conducted using a Philips PW1050 X-ray diffractometer. There was a range of 2.5 to 10 in the diffraction angle (2) [28].

2.4.7 Energy dispersive x-ray spectroscopy (EDX)

The EDX examination of activated carbons is to estimate the distribution and content of elements of the Carbon samples. The analysis was carried out at a 9 mm working distance and an accelerating 20 kV voltage. To guarantee homogeneity, X-ray spectra were obtained from several areas of the material. Using semi-quantitative analysis, the obtained spectra were analysed using (EDAX Genesis) to determine the elements present based on their distinctive X-ray peaks and to estimate their relative concentrations [28].

2.5 Kinetic and equilibrium adsorption studies

At ambient temperature, prepared activated carbon was subjected to batch adsorption of Fe^{3+} from the water solution. Fe^{3+} solution was mixed with a specific amount of adsorbent and using rotary orbital shaker it was shaken at 150 rpm. Following a certain amount of contact time, the mixture was filtered through Whatman-42 filter paper. This study used an adsorption spectrophotometer (AAS) to analyse the adsorbent dosage effects, effect of initial metal ion concentration, solution pH, and contact time for quantification of the extent of adsorption. The optimization was done using batch tests where the solution pH (2, 4, 6, 8, 10,

12), optimum time (15, 30, 45, 60, 75, 90 min), optimum dose (0.01, 0.02, 0.03, 0.04, 0.05, 0.06, 0.07, 0.08 g), and initial concentration (5, 6, 7, 8, 9 and 10 mg/L) were varied. The following formula was used to estimate the activated carbon's adsorption capacity (mg/g) [26, 29].

$$\text{Adsorption capacity} = \frac{C_o - C_i}{C_o} \times \frac{V}{W} \quad (1)$$

$$\text{Removal sorption}\% = \frac{C_o - C_i}{C_o} \times 100 \quad (2)$$

here initial and equilibrium Fe^{3+} concentration in mg/L are denoted by C_o and C_i respectively, mass of the adsorbent is demarcated by W in g and the solution volume V in L.

3 Results and discussion

3.1 Characterisation of raw material and activated carbon

3.1.1 Calorific value

The calorific value of horse chestnut shell, after evaluation using a bomb calorimeter revealed that upon complete combustion, sample has a calorific value of approximately 15 MJ/Kg. This value, obtained through precise measurements in the bomb calorimeter, indicates that 1 gram of chestnut shell releases 15 mega joules of heat energy when burned. The relatively high calorific value of chestnut shell makes it an attractive renewable fuel source for various applications, such as domestic heating, industrial boilers, or co-firing with coal in power plants. Accurate determination of the calorific value is crucial for optimizing the energy conversion efficiency and economic viability of utilizing horse chestnut shell as a biofuel [30, 31].

3.1.2 Thermogravimetric analysis

Thermogravimetric analysis (TGA) in a nitrogen environment was used to evaluate the thermal stability of the activated carbon made from horse chestnut shells. Different phases of weight loss corresponding to various heat events in the sample are shown by the TGA curve in Fig. 2. The evaporation of moisture and the elimination of physically adsorbed water are the main causes of the initial weight loss between 30 and 150 $^{\circ}\text{C}$, reflecting the moisture content of the sample. The primary organic components of the horse chestnut shell, hemicellulose, cellulose, and lignin, decompose between 150 and 350 $^{\circ}\text{C}$, causing a notable weight loss of roughly 40%. In the process, volatile chemicals are released and a thermally stable carbon structure is created. The sample exhibits negligible weight loss up to

900 °C above 350 °C, suggesting that the residual material is primarily carbonaceous and has a high degree of heat stability—a quality crucial to its efficacy as an adsorbent in high-temperature applications. The effectiveness of the carbonisation and activation procedures in eliminating non-carbon components and forming a stable carbon structure is confirmed by this research [26, 32].

3.1.3 The activated carbons surface characteristics

The BET test was conducted to evaluate the surface area and pore size, and pore diameter of the prepared activated carbons. The temperature of activation is the prime criterion for the process. The effects of activation temperature, surface area, and total pore volume were investigated at a ratio of three for the KOH/horse chestnut shell impregnation. As the temperature rose from 650 °C to 750 °C, the surface area showed increment from 370.528 to 685.808 m²/g. According to the International Union of Pure and Applied Chemistry (IUPAC) classification system, the HCAC showed a type (IV) isotherm, suggesting that it is a mesoporous solid [33]. The trend was consistent for both the micro pore volume and the total pore volume. An improved development of developed porosity in the raw material is a result of increasing the temperature of activation to 750 °C. The concentration of KOH increases this action, suggesting that this temperature is appropriate for the evolution of

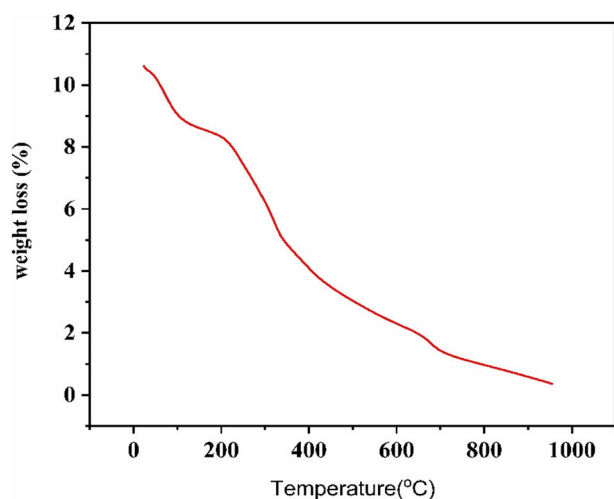


Fig. 2 TGA of horse chestnut shell

porosity. The prepared sample has the potential to be an adsorbent due to its physicochemical features [26, 32]. Table 2 elaborates the prepared activated carbons surface characteristics and Table 3 gives the comparison of various activated carbons with the prepared activated carbon using horse chestnut shell in terms of specific surface area. Furthermore, the N₂ adsorption-desorption isotherms of the developed activated carbons are displayed in Fig. 3. The adsorption isotherm shape provides quality information about the process of adsorption and the surface area that is accessible to the adsorbate. It is possible to conclude that all prepared activated carbons displayed steep type iv from the isotherm forms. The adsorption-desorption isotherms show a sharp increment at low relative pressures, which is accompanied by an early horizontal plateau at high relative pressures, suggesting the existence of extremely microporous materials. The lack of a hysteresis loop meant that there was little to no mesopore in the carbon products, which were primarily composed of micropores [29].

3.1.4 SEM evaluation of horse chestnut shell and activated carbon

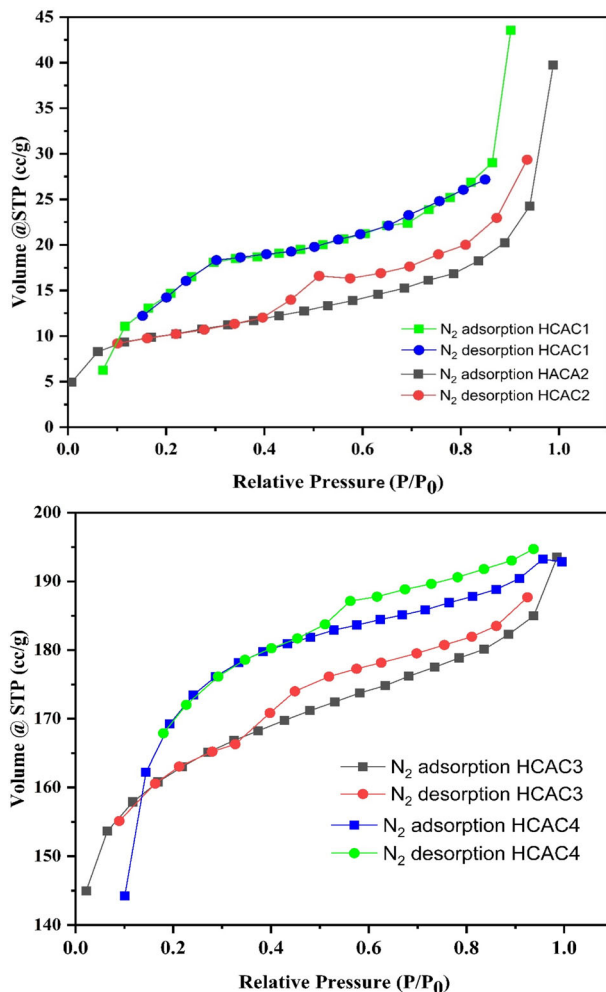
Using a SEM, the surface characteristics of the prepared activated carbons and the horse chestnut shell were examined. The manufactured activated carbons named as horse chestnut activated carbon and written as (HCAC1, HCAC2, HCAC3, and HCAC4) and the horse chestnut shell and activated carbon SEM images before Fe³⁺ adsorption are provided in Fig. 4a (raw chestnut shell), b (impregnation ratio 1 and temperature 650 °C), c (impregnation ratio 1 and temperature 750 °C), d (impregnation ratio 3 and temperature 650 °C), and e (impregnation ratio 3 and temperature 750 °C), respectively and after Fe³⁺ adsorption are provided in Fig. 4f (impregnation ratio 1 and temperature 650 °C), g (impregnation ratio 1 and temperature 750 °C), h (impregnation ratio 3 and temperature 650 °C), and i (impregnation ratio 3 and temperature 750 °C), respectively. The chestnut shell has a smooth surface. The shell surface is not very much textured, and it is less porous. This would explain its low BET surface area. However, pore structure of the activated carbon's was able to be enhanced by the activation procedure. With an impregnation ratio of one and three, the activated carbon produced at 650 °C and 750 °C exhibits a good and successful pore development. It appears to

Table 2 Surface properties of the Activated Carbon

AC Samples	Impregnation ratio	Activation temperature (°C)	SBET (m ² /g)	V Micro (cc/g)	V Meso (cc/g)	V(total) (cc/g)	Dp (nm)
AC 1-650	1	650	180.768	0.005	0.11	0.115	3.895
AC 1-750	1	750	628.857	0.188	0.17	0.358	1.694
AC 3-650	3	650	370.528	0.02	0.29	0.31	3.951
AC 3-750	3	750	685.808	0.22	0.32	0.54	1.699

Table 3 Comparison of SB_{et} for various activated carbons produced from different biomass

S.no	Biomass	Activating agent	Temperature	Specific surface area (m^2/g)	Reference
1	Guava peel	H_3PO_4	600	471.3	[37]
2	Sewage sludge-derived	KOH	600	172	(Nunthaprechachan et al., 2013)
3	Coir pith	H_2SO_4	650	598	(Santhy and Selvapathy, 2004)
4	Apricot stones	H_3PO_4	750	359.4	(Djilani et al., 2015)
5	Macore fruit	NaOH	700	229.51	[36]
6	Peanut sticks wood	HCL	750	218.89	(Ghaedi et al., 2014)
7	Avocado peel		600	452	[35]
8	Rice husk	H_2SO_4	650	98.27	(Kalderis et al., 2008)
9	Palm shell waste	NaOH	700	731.50	(Wong et al., 2016)
10	Horse chestnut shell	KOH	750	685	-

**Fig. 3** N₂ adsorption-desorption isotherms of prepared activated carbons

have a comparatively large surface area because of its highly porous and irregular surface. Following iron (Fe^{3+}) adsorption, SEM images showed significant morphological changes in the activated carbon. The surface was rough and porous at first, suggesting a large concentration of active sites. The surface showed less porosity and a smoother appearance after adsorption, indicating that iron ions had taken up residence in the pores. Small clusters on the surface provided additional evidence of the material's successful iron adsorption and demonstrated how well it removed iron from aqueous solutions [34]. The surface area calculated using BET is shown in Table 2, and it supports this observation.

3.1.5 FTIR spectra of activated carbon

Both porosity and the surface's functional groups chemical reactivity affect activated carbon's ability to adsorb substances. Understanding surface functional groups would help to understand the created activated carbons capacity for adsorption [35]. The before and after adsorption FTIR spectrum of four activated carbons (HCAC1, HCAC2, HCAC3, and HCAC4) that were prepared at two temperatures and two impregnation ratios are shown in Fig. 5a and 5b respectively. In Fig. 5a the vibrations stretching at 3500–4000 cm^{-1} indicate the existence of OH groups of alcohols, phenols, and carboxylic acid in all four activated carbons [36]. The methylene group ascertained by C-H stretching at a wave number of 2960 cm^{-1} in HCAC2 while it was noticed at 2890 cm^{-1} , 2931 cm^{-1} in HCAC3, and HCAC4, respectively [37]. The band seen at 2360–2361 cm^{-1} correlates to the C–O stretching vibration for carbon monoxide or carbon dioxide derivatives in HCAC3, and HCAC4 [38]. The presence of N–H (bend), which denotes the presence of a secondary amide group in tall activated carbons, was revealed by vibrations at 1500–1700 cm^{-1} [39]. The

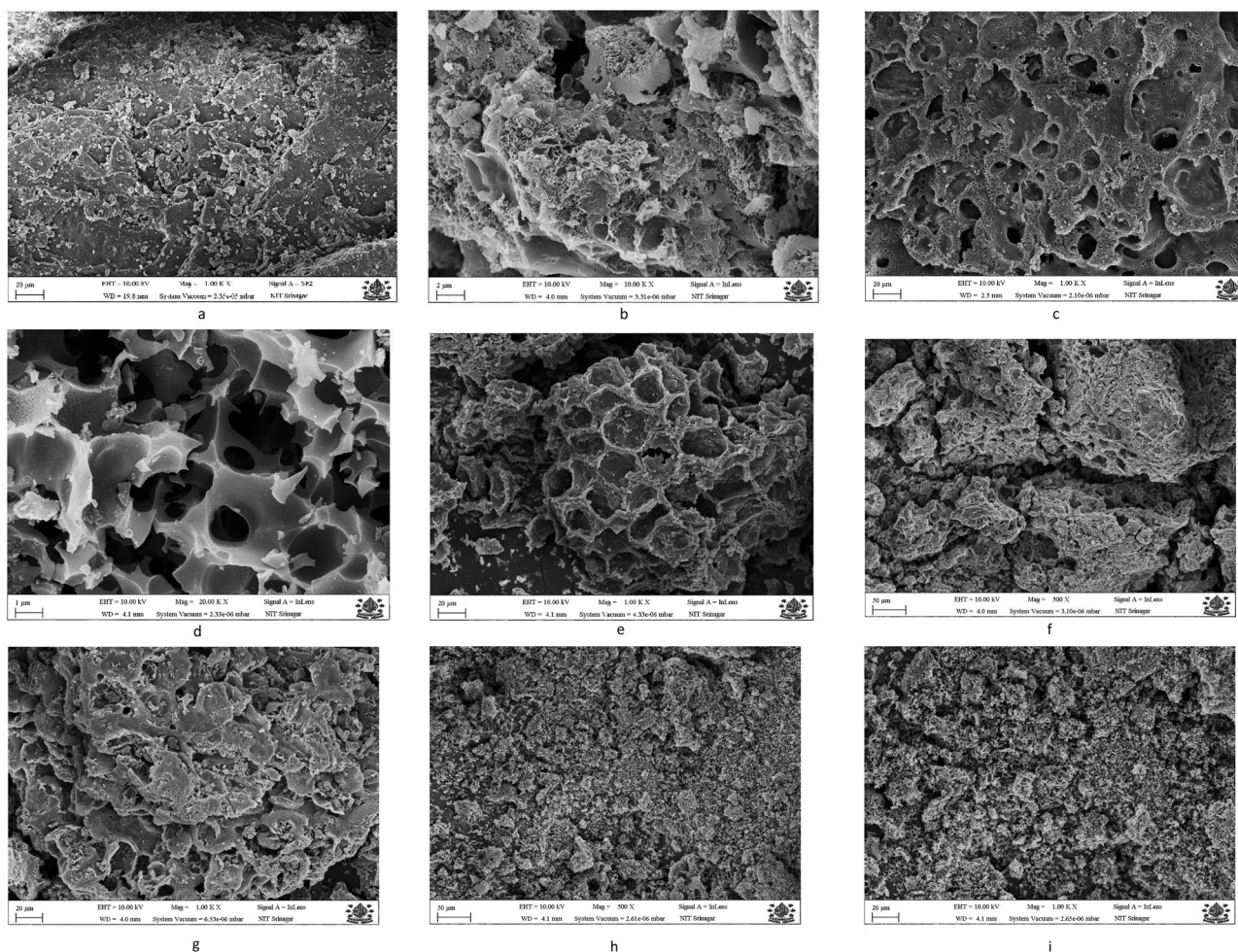


Fig. 4 Sem images of prepared activated carbon before Fe^{3+} adsorption. **(a)** Raw horse chestnut shell. **(b)** Impregnation ratio 1 at 650°C . **(c)** Impregnation ratio 1 at 750°C . **(d)** Impregnation ratio 3 at 650°C . **(e)** Impregnation ratio 3 at 750°C . **(f)** Impregnation ratio 1 and

temperature 650°C , **(g)** Impregnation ratio 1 and temperature 750°C , **(h)** Impregnation ratio 3 and temperature 650°C , and **(i)** Impregnation ratio 3 and temperature 750°C

existence of chloride (Cl) is guaranteed by the peak intensities at 718.46 cm^{-1} , 825.03 cm^{-1} , 987.21 cm^{-1} , and 967.34 cm^{-1} in HCAC1, HCAC2, HCAC3, and HCAC4 correspondingly. However, in Fig. 5(b) that is after adsorption the FTIR analysis reveals notable changes that points to interactions between the functional groups on the activated carbon surface and the Fe^{3+} ions [17]. The shift and intensity of key peaks associated with hydroxyl ($-\text{OH}$), carbonyl ($\text{C}=\text{O}$), and carboxyl ($-\text{COOH}$) groups indicate their involvement in binding Fe^{3+} ions; the broad $-\text{OH}$ peak around 3400 cm^{-1} is reduced, and the carbonyl peak near 1700 cm^{-1} is shifted, indicating that these groups take part in chemisorption and form stable bonds with the Fe^{3+} ions during adsorption [40].

3.1.6 Energy dispersive x-ray spectroscopy (EDX)

Produced activated carbons has enormous utilisations, like catalysis, purification, storage of energy, and adsorption of gas, taking into account its large surface area and good

carbon content [41]. Table 4a and b shows the elemental analysis data (EDX) of the prepared activated carbons before and after iron adsorption. EDX analysis shows the presence of K in the activated carbon which confirms the activation agent KOH that has been used during the process. The EDX imaging of the activated carbons revealed the presence of several elements, including carbon, oxygen, magnesium, aluminium, phosphorus, and potassium. The carbon present in HCAC1, HCAC2, HCAC3, HCAC4 before Fe^{3+} adsorption is 66.5%, 72.8%, 87.1% and 88.4% respectively. All the samples have majorly carbon present in them which indicates the successful preparation of activated carbon from the biomass (horse chestnut). Since other elements present are very less thus confirming very little impurity in it. After adsorption of Fe^{3+} the EDX imaging of the activated carbons revealed the presence of the Fe in addition to the other elements which proves that the adsorption of Fe has taken place on the activated carbon [17].

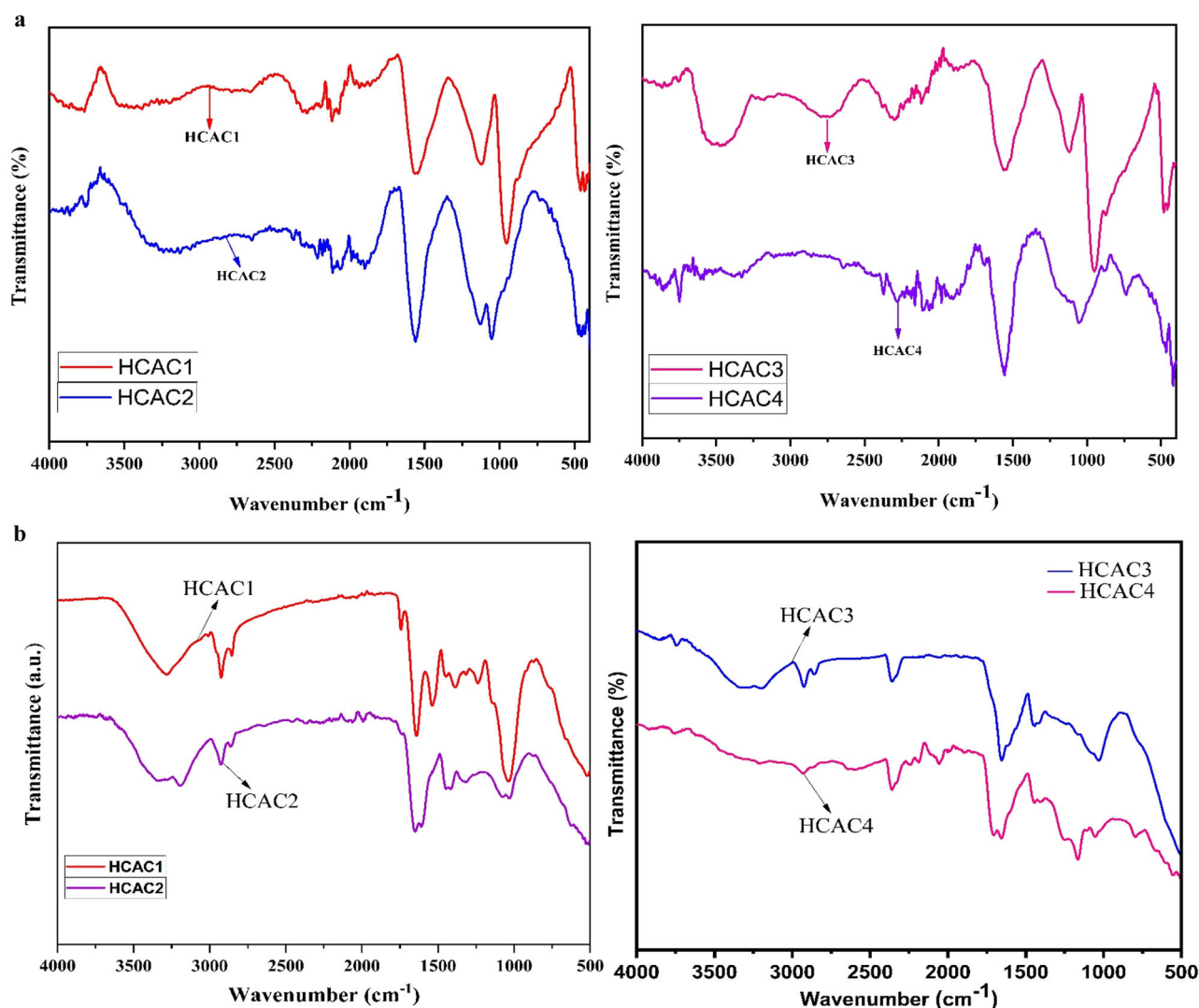


Fig. 5 a FTIR pattern of derived activated carbon before adsorption. b FTIR pattern of derived activated carbon after adsorption

Table 4 a EDX elemental analysis of produced activated carbons. b EDX elemental analysis of produced activated carbons after Fe^{3+} adsorption

Element	HCAC1 (Weight %)	HCAC2 (Weight %)	HCAC3 (Weight %)	HCAC4 (Weight %)
a				
C K	66.5	72.8	87.1	88.4
O K	26.3	21.8	11.8	10.4
Mg K	0.2	0.2	0.2	0.2
Al K	2.9	1.0	0.1	0.2
P K	0.3	0.3	0.3	0.3
K K	3.7	3.9	0.5	0.4
b				
C K	56.3	66.2	76.2	77.6
O K	20.7	17.7	8.2	7.2
Mg K	0.2	0.2	0.2	0.2
Al K	2.3	1	0.1	0.2
P K	0.3	1.0	0.3	0.3
K K	3.2	0.3	0.5	0.4
Fe K	10.05	11.36	18.47	24.21

3.1.7 X-ray diffraction analysis (XRD)

The X-ray diffraction (XRD) patterns of the four activated carbons manufactured by KOH activation (HCAC1, HCAC2, HCAC3, and HCAC4) before and after adsorption are shown in Fig. 6a and b. As shown in Fig. 6(a) all samples show a clear peak at about $2\theta = 25^\circ$, which is located in the (002) plane of the carbonaceous structure and indicates the existence of amorphous, disordered carbon (Thirumal et al. 2022). The termination of double bonds with hydrogen atoms, which prevents the production of a highly ordered structure, is responsible for the amorphous aspect of the activated carbon made using KOH (Xu et al. 2014; Lazzarini et al. 2016). Among the samples, HCAC4 shows a more prominent peak with a centre at 25.5° , which is typical of activated carbon that is graphitic and indicates a minimal degree of crystalline order and graphitization. In Fig. 6b that is after adsorption of Fe^{3+}

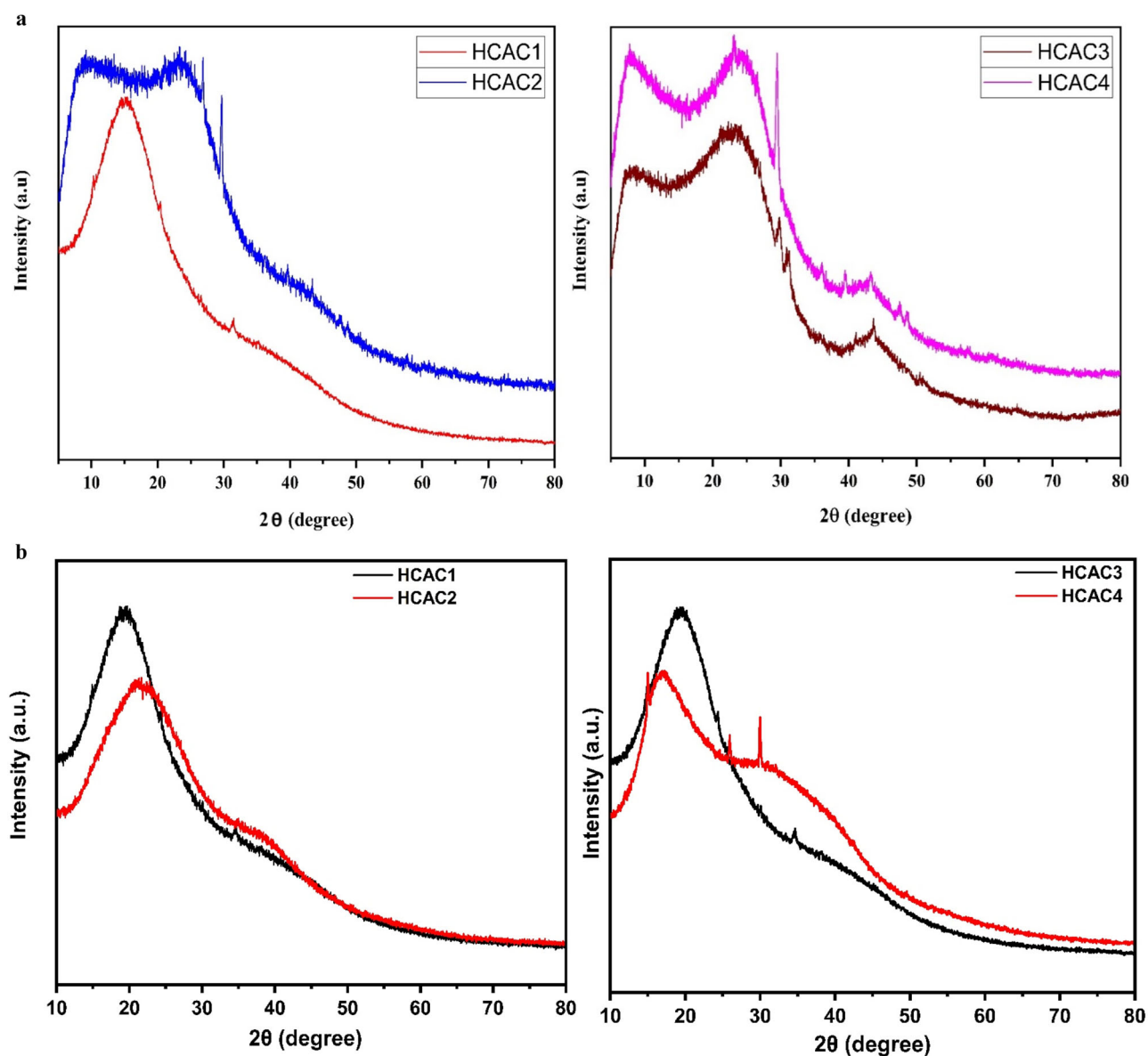


Fig. 6 **a** XRD pattern of the prepared activated carbons before Fe^{3+} adsorption. **b** XRD pattern of the prepared activated carbons after Fe^{3+} adsorption

there is a slight decrease in the intensity of the highly organised peaks following the adsorption of ferrous ions. This has been linked to the ferrous ion's adsorption on the top layer of the carbon surface's crystalline structure.

The Scherrer equation was used to examine the crystallite size of the graphitic domains in activated carbons in more detail:

$$D = \frac{K\lambda}{\beta \cos \theta} \quad (3)$$

where D is the crystallite size, K is the form factor (usually 0.9), λ is the X-ray wavelength (usually 0.15406 nm for $\text{Cu K}\alpha$ radiation), θ is the Bragg angle, and β is the full width

at half maximum (FWHM) of the peak in radians. The HCAC4 sample's computed average crystallite size was 4.4 nm and it supports the material's mostly amorphous structure and small graphitic domains, demonstrating how well KOH activation creates a very porous material with little crystalline order. Likewise, the average computed crystalline size of HCAC1, HCAC2 and HCAC3 was found out as 7.5 nm, 6.3 nm and 5.6 nm respectively.

3.2 Kinetic studies

The activated carbon that has highest surface area which happens to be HCAC4 in the present study was used in

adsorption and kinetic studies. To examine the rate data and study if the adsorption process mechanism or chemical reaction controls its rate, an appropriate kinetic model is required. Numerous models, including the pore diffusion model, heterogeneous diffusion model, and homogeneous surface diffusion model, have been widely employed to explain how adsorbates are transported inside of adsorbent particles. The kinetics of Fe^{3+} adsorption onto activated carbon are modelled using the pseudo-1st-order, pseudo-2nd-order, and intraparticle diffusion model in order to explore the governing mechanism of the processes of adsorption.

3.2.1 Pseudo first-order reaction

Pseudo-first-order kinetic model was proposed by Lagergren, the pseudo-1st-order kinetic model's linear form is illustrated below [42].

$$\text{Log}(q_e - q_t) = \log q_e - \frac{k_1 t}{2.303} \quad (4)$$

where the concentration of Fe^{3+} adsorbed in (mg/g) at balance point and any given time t is written as q_e and q_t , respectively, and k_1 signifies the rate constant of adsorption (h^{-1}). The pseudo first order adsorption kinetics are plotted as $\log(q_e - q_t)$ versus t , providing a straight line that may be used to calculate the rate constant k_1 (Fig. 7a). The estimated linear regression correlation coefficients (R^2) were rather small, at 0.76, and the computed values generated from the linear plots did not agree with the experimental q_e values. The value of K_1 was calculated as 0.00053 and the values of q_e and q_t was found as 80.525 and 3.49 respectively.

3.2.2 Pseudo second order reaction

The expression of pseudo-2nd-order rate is another popular kinetic expression. The pseudo-2nd-order rate formula has the following linear structure [43, 44]:

$$\frac{t}{q_t} = \frac{1}{k_2 q_e^2} + \frac{t}{q_e} \quad (5)$$

where k_2 signifies the rate constant of pseudo-second-order reaction (g/mg min), and the amounts of Fe^{3+} adsorbed (mg/g) at equilibrium and at time t (min), are denoted by q_e and q_t respectively. The plot of t/q_t versus t (Fig. 7b) which is slope and intercept can be used experimentally to calculate capacity of the adsorption at equilibrium (q_e) and the second order constants (k_2). Table summarizes the values of the computed linear regression correlation coefficient and q_e , k_2 . The values of R^2 , K_2 , q_e as per the table are 0.9923, 0.0028 and 83.75 respectively.

3.2.3 Intraparticle diffusion model

The process of solute movement inside porous adsorbents, like activated carbon, is theoretically explained by the intraparticle diffusion model. The intraparticle diffusion rate equation is represented as; [39]

$$q_t = k_p t^{1/2} + C \quad (6)$$

where k_p signifies the intra-particle diffusion rate constant ($\text{g mg}^{-1} \text{min}^{-0.5}$) and its value is 8.317. In any event if the rate-restricting step is solely intraparticle diffusion, the origin is crossed by the q_t vs $t^{1/2}$ plot. when the origin is not traversed by the plot, there may be a control of boundary layer present. This further demonstrates that other kinetic models, which might be active at the same time as the step of intra-particle diffusion, could be in charge of the rate of adsorption in addition to the diffusion step. The value of R^2 is 0.8463.

By analysing Fig. 7a–c it is seen that the linear plot of pseudo first order and intraparticle diffusion does not pass through origin and there (R^2) value is also relatively low when compared to second order reaction whose (R^2) value is 0.99. The values of the constants are summarized in Table 5. The second-order kinetic model for Fe^{3+} adsorption may be a more favourable approximation of the adsorption kinetics. These findings imply that the pseudo-second-order kinetic mechanism is more likely to be at play and that the rate-limiting phase that regulates the adsorption process may be chemisorption. Other workers also experienced similar outcomes [45–47].

3.3 Adsorption studies with various isotherm model

Isotherm models were employed to improve comprehension of capacity of the adsorption and provide a more convincing account of the adsorptive process by the adsorbent. The highly prominent isotherm model, that primarily elaborates the connection among the adsorbent and adsorbate, is also unravelled by the adsorption isotherms research [48, 49]. Therefore, to characterise the sorption of Fe^{3+} on HCAC4, isotherm models such as the Langmuir, Freundlich, Temkin, Dubinin-Radushkevich, Harkin Jura, and Halsey isotherms were used [50]. Table 6 provides the equilibrium isotherm parameters.

3.3.1 Langmuir adsorption isotherm

As per this isotherm, adsorption occurs at particular homogenous locations in the adsorbent. The linear form of this isotherm is provided as [51]

$$\frac{1}{q_e} = \frac{1}{K_1 q_{\max}} \times \frac{1}{C_e} + \frac{1}{q_{\max}} \quad (7)$$

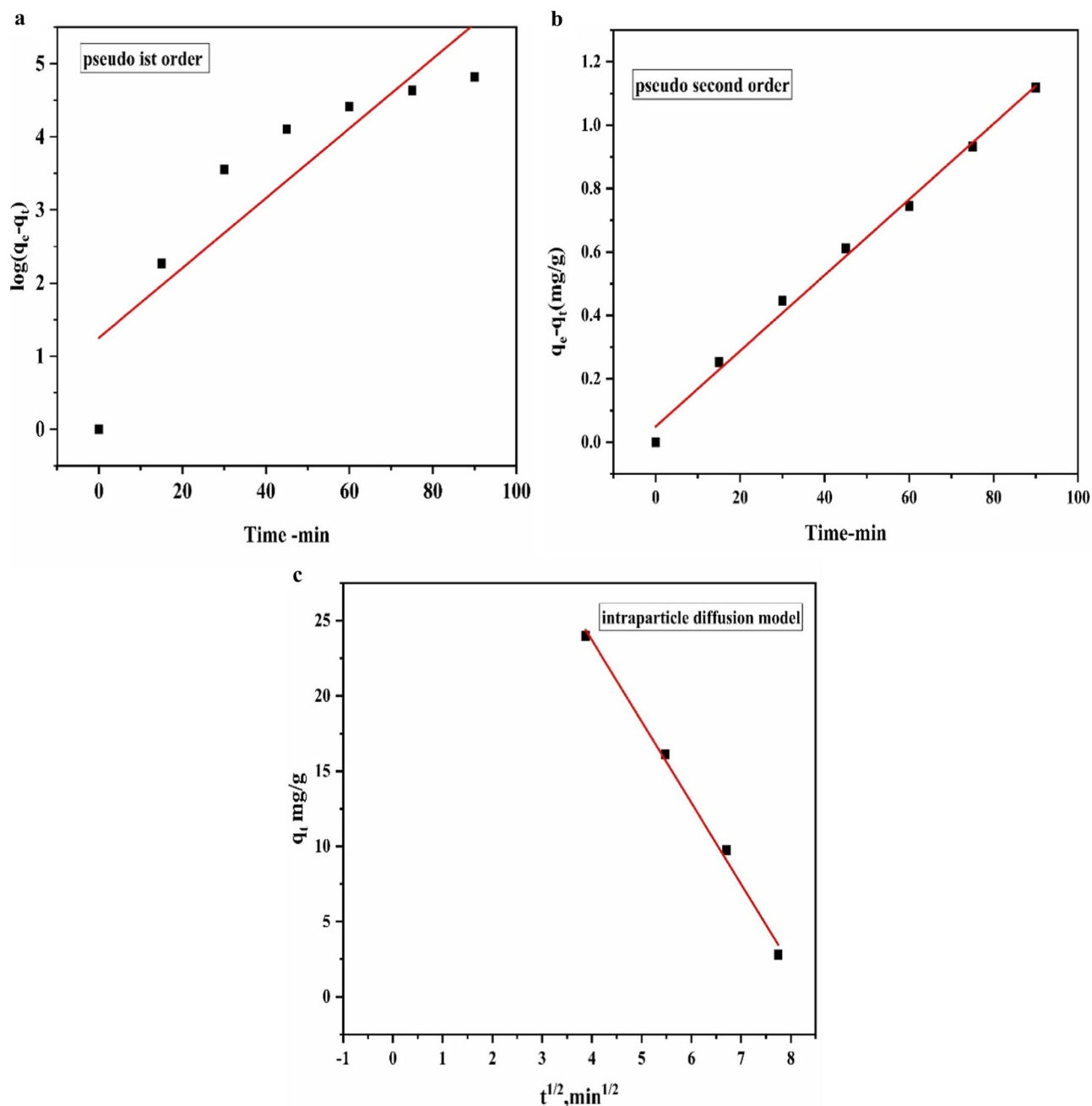


Fig. 7 Linear Kinetic plots for Fe adsorption (a) pseudo first order (b) Pseudo second order (c) intraparticle diffusion model

Table 5 Kinetic parameters for adsorption rate expression

First order kinetic reaction				Second order kinetic reaction				Intraparticle diffusion model	
q_e (exp)	K_1 (1/min)	q_e (cal) mg/g	R^2	K_2 (g/mg min)	q_e (cal) mg/g	R^2	K_p (mg/g min ^{1/2})	R^2	
80.525	0.00053	3.49	0.7611	0.0028	83.75	0.9923	8.317	0.8463	

where the adsorbed amount of Fe^{3+} on prepared activated carbon (mg/g) is denoted by q_e , the concentration of equilibrium is denoted by C_e in (mg/L), K_1 signifies

equilibrium constant (L/mg), and maximum adsorption capacity is given by q_{\max} . The coefficients of adsorption are displayed in Fig. 8a as a plot of C_e/q_e against C_e . Based on a

Table 6 Isotherm parameters for the removal of Fe³⁺

Models	Parameters	
Langmuir	q _{max}	141.043
	q _e	132.166
	K _l	106851
	R ²	0.99
Freundlich	1/n	0.199
	K _f	114.34
	R ²	0.986
Temkin	B _t	20.72
	K _t	262.27
	R ²	0.983
Halsey	n _H	5.02
	K _h	30790
	R ²	0.986
Dubinin Radushkevich	Energy (Kj/mol)	12390
	R ²	0.98
Harkin Jura	A	9.22432 × 10 ⁻⁵
	B	7.94011 × 10 ⁻⁵
	R ²	0.95

dimension-less equilibrium parameter, the Langmuir equation can be further analysed. A favourable adsorption is accomplished if the mean of the K_l values fall within the concentration range of 0 and 1.

3.3.2 Freundlich adsorption isotherm

This isotherm assumes a surface with an uneven heat of adsorption distribution over the surface. Its linear form can be represented by:

$$\log q_e = \log k_f + \frac{1}{n} \log C_e \quad (8)$$

where the adsorption capacity (mg/g) is denoted by q_e, C_e signifies the concentration at equilibrium of the Fe³⁺ solution (mg/L), and k_f represents adsorption capacity and n represent and adsorption intensity both are Freundlich constants. The value k_f and n is shown in Table 6 and were derived from the slope and intercept of a plot of log q_e vs log C_e (Fig. 8b).

3.3.3 Temkin and Pyzhev adsorption isotherm

Temkin and Pyzhev examined how adsorption isotherms were impacted by indirect adsorbate/adsorbent interactions. The heat of adsorption of each molecule in the layer would decrease linearly with coverage due to adsorbate/adsorbent interactions. The Temkin isotherm's linear form can be written as [52, 53]

$$q_e = B \ln A + B \ln C_e \quad (9)$$

where B is associated with the heat of adsorption, A is the equilibrium binding constant (L/mg), and B = RT/b. The plot of q_e against ln C_e (Fig. 8c) makes the isotherm constants determinable. Table 6 included the Temkin isotherm constants. Table 6 provides the values of the correlation coefficients and isotherm constants.

3.3.4 Halsey isotherm model

When assessing multilayer adsorption at a considerable distance from the surface, the Halsey isotherm is utilized [52, 54]. The Halsey adsorption isotherm is represented as follow

$$q_e = \frac{1}{n_H} \ln K_H + \frac{1}{n_H} \ln C_e \quad (10)$$

where the slope and intercept of the plot of ln q_e versus ln C_e yield the Halsey isotherm constants, K_H and n_H. Figure 8d illustrates how well the Halsey isotherm (high correlation coefficient value, R²) of 0.982 fits the experimental data. As a result, the results may be explained by the large multilayer sorption activity on the activated carbon surface and the heterogeneous distribution of active sites.

3.3.5 Dubinin-Radushkevich isotherm

Use of this isotherm model allowed for the separation of the chemical and physical aspects of the sorption of the Fe³⁺ ion onto activated carbon. The following is a linear representation of the model.

$$\ln q_e = \ln q_{\max} - K \epsilon^2 \quad (11)$$

where q_e is the starting concentration and q_{max} is the adsorption capacity. Using the intercept and slope data, a plot of ln q_e versus ε was created to calculate the values of R² (0.98) and energy E (1239 KJ/mol). (shown in Fig. 8e) [54].

3.3.6 Harkin Jura isotherm

In this Isotherm model the multilayer sorption of Fe³⁺ is assumed to occur within a heterogeneous pore distribution. Based on the formula

$$\frac{1}{q_e^2} = \frac{B}{A} - \left(\frac{1}{A}\right) \log C_e \quad (12)$$

where B and A are isotherm constants that are evaluated from plotting 1/q_e² versus log C_e, the plot of 1/q_e² vs log C_e is shown in Fig. 8f. After calculating the values of the intercept and slope, the Harkin Jura constants A, B, and R² were determined to be 0.273 mg /g, 0.09, and 0.782.

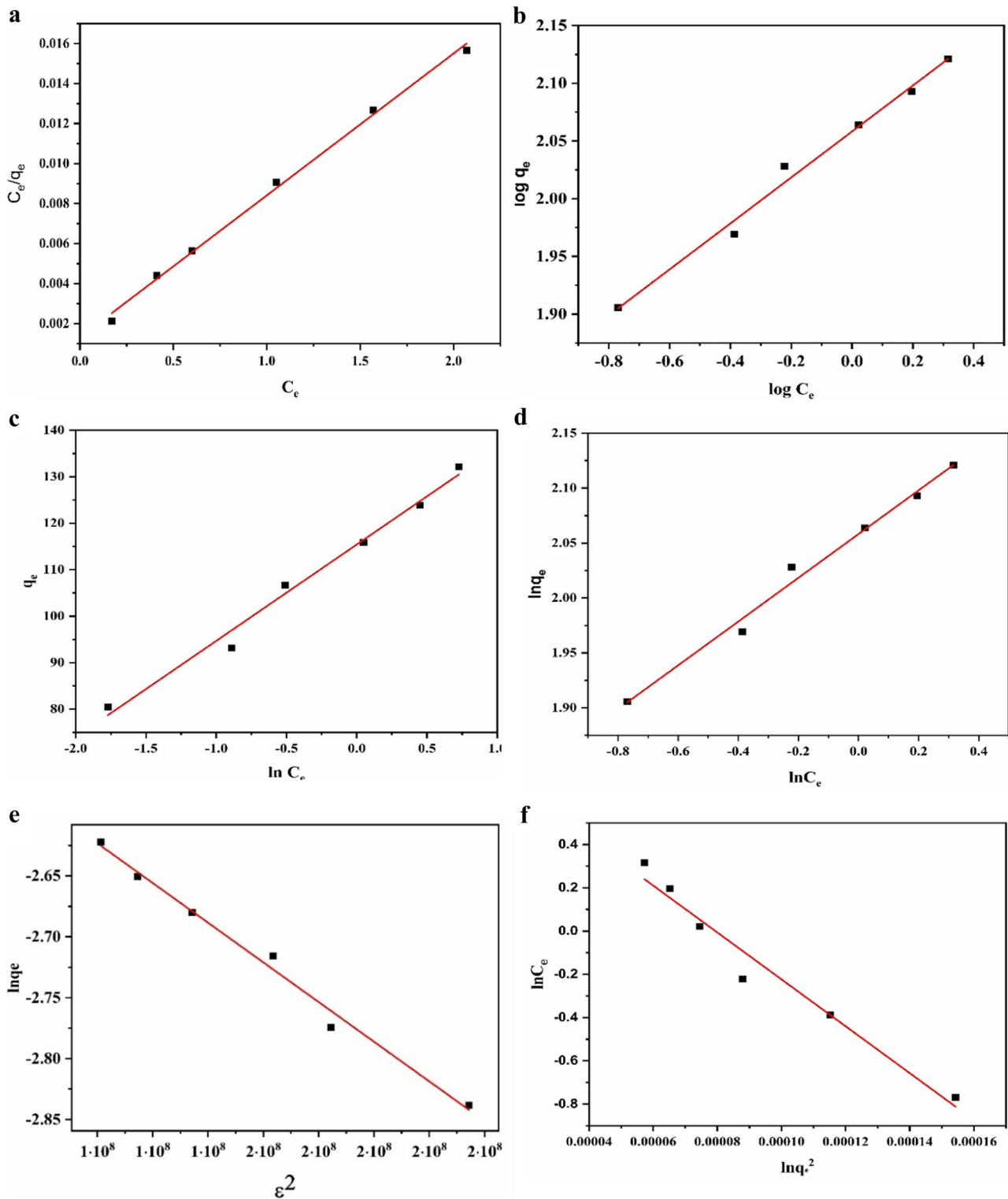


Fig. 8 Linear adsorption isotherms for adsorption of iron. **a** Langmuir isotherm. **b** Freundlich isotherm. **c** Temkin isotherm. **d** Halsey isotherm. **e** Dubinin and **f** Harkin jura

With an R^2 value of 99.5, the Langmuir isotherm model demonstrated the maximum sorption of Fe^{3+} ions onto HCAC4. Therefore, the assumption that the surface is

homogenous, indicating a homogeneous spread of sorption sites on the activated carbon, is the most appropriate model for explaining the sorption of Fe^{3+} ions onto HCAC4. As a

Table 7 Comparison of Langmuir q_{\max} with other activated carbons

S.no	Biomass	Langmuir q_{\max} (mg/g)	Reference
1	Pecan shell	41.66	[34]
2	Bombax ceiba fruit	37.16	[17]
3	Liminia Acidissima	3.681	(R. Pohling, <i>Chemische Reaktionen in der Wasseranalyse</i> , Springer Spektrum, 2015)
4	Nigerian Bamboo	166.7	(Arivoli et al., 2013)
5	Thespesia populnea	141.81	(Prabakaran and Arivoli, 2011)
6	Jambul bark	0.198	(Rose and Rajam, 2012)
7	Wild jack	0.257	(Rose and Rajam, 2012)
8	Horse chestnut shell	138	Present study

result, Fe^{3+} ions were absorbed as monolayer coverage on the surface of activated carbon, which has a significant number of uniformly energy-dense sorption sites. As a result, according to the R^2 value, the isotherm Fe^{3+} ion adsorption by HCAC4 activated carbon is more fit than Freundlich, Halsey, Temkin, Dubinin-Radushkevich, and Harkin Jura. The adsorption capacity of HCAC4 towards Fe^{3+} (138.88 mg/g) turned out to be the greatest while comparing with other adsorbents. Table 7 gives the comparison of q_{\max} values of some activated carbons with HCAC4.

3.4 Effects of process parameters that influences adsorption

3.4.1 Effect of pH

The degree of metal adsorption process is significantly influenced by the initial pH of the contact solution. The pH of the contact solution affects both the surface charges of the adsorbent and the availability of metal ions [55]. For the verification of the effect of pH for the removal of Fe^{3+} using HCAC4, the effect of pH of the solution was carried out by altering the pH from 2 to 12 at a difference of 2 for 1000 mL of 5 mg/L solution, where the adsorbent dose was 0.06 g at an agitation speed of 150 rpm for 60 min of contact time. This pH range was chosen to avoid the formation of insoluble metal hydroxide precipitates. The adsorption of Fe^{3+} was found to be maximum (96.63%) at pH 6. Figure 9a shows the effect of pH and percentage removal. It was seen that initially the increment of the pH increased the removal efficiency and after the pH reached 6 the removal percentage started decreasing. At low pH (below pH_{pzc}), the charge on the surface of activated carbon was positive, so electric repulsion between the cation and activated carbon occurs which becomes the reason for low adsorption values. Additionally, the competition between H^+ and Fe^{3+} for adsorption at ion-exchangeable sites of carbon will be high in acidic medium this leads to least metal ion removal. With

increment in pH i.e beyond (pH_{pzc}) the successive deprotonation of positive charged groups and unprotonated carboxyl groups present at the surface of the activated carbon increases the surface density of negative charge and also lowers the H^+ ion concentrations. This results in electrostatic attraction among adsorbents negatively charged sites and rise in the cationic charge. The amount of Fe^{3+} adsorption increases with increase in pH from 2 to 6 and then decreases from 6 to 8. This decrease in adsorption is mainly due to development of soluble hydroxyl groups [56, 57]. Figure 10 shows the pH_{pzc} and its value was 5.6 which means the shift of charge occurs at 5.6 of pH value.

3.4.2 Effect of initial concentration

When employing activated carbon to remove heavy metal from wastewater, the starting concentration is a crucial factor as well. The experiment involved altering the starting Fe^{3+} concentrations (5 mg/L, 6 mg/L, 7 mg/L, 8 mg/L, 9 mg/L, and 10 mg/L) of 1 L FeCl_3 solution while keeping pH 6 and adsorbent dosage of 0.06 g. The elimination of Fe^{3+} was observed utilizing the manufactured activated carbon. For sixty minutes, the solution was stirred at 150 rotations per minute Fe^{3+} elimination reached its peak (96.62%) at 5 mg/L of concentration. The findings show that when the amount of sorbent in the system increased, more Fe^{3+} was extracted from the solution. The availability of a larger surface area on the activated carbon surface with a higher number of functional groups could account for this result [57]. Also at low iron /carbon ratio the adsorption of iron ions occurs on high energy sites and when the iron/carbon ratio increases the saturation of these high energy sites occur and adsorption process begins at low energy sites thereby decreasing the adsorption efficiency Fig. 11.

3.4.3 Effect of adsorbent dosage

The dosage of the adsorbent is one of the most important parameters in the removal of heavy metals from wastewater.

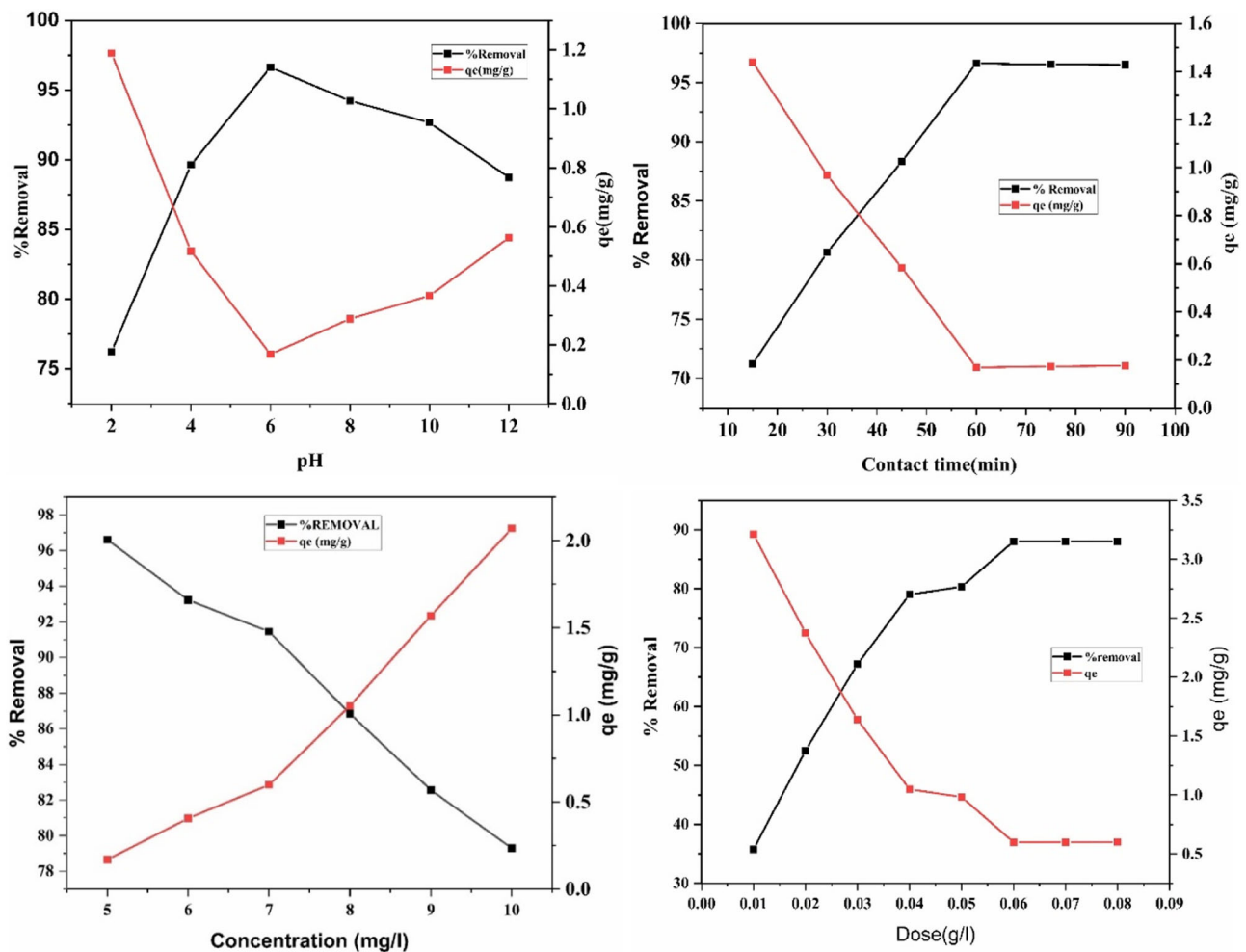


Fig. 9 Effect of pH, contact time, initial concentration, adsorbent dose on iron removal % using HCAC4

The prepared activated carbon was used to remove Fe^{3+} from a 5 mg/L, 1 L FeCl_3 solution. The dose of the activated was adjusted to range from 0.01 to 0.08 g, with a variation of 0.01 g. The pH of the solution was maintained at 6, and it was agitated for 60 min at a speed of 150 rpm. The greatest significant Fe^{3+} elimination (88.04%) was noted with a 0.06 g activated carbon dosage. The effect of adsorbent dosage and percentage removal is depicted in Fig. 9. It was observed that when the dose was increased, the removal efficiency rose initially. However, the removal % began to decrease when the dose reached 0.06.

3.4.4 Effect of contact time

The duration of contact between the metal solution and the adsorption surface affects the percentage of metal removal. The study involved optimizing the contact time for the removal of Fe^{3+} using horse chestnut shell activated carbon in a 1 L solution containing 5 mg/L Fe^{3+} . The adsorbent dosage was 0.06 g, and the solution pH was maintained at 6

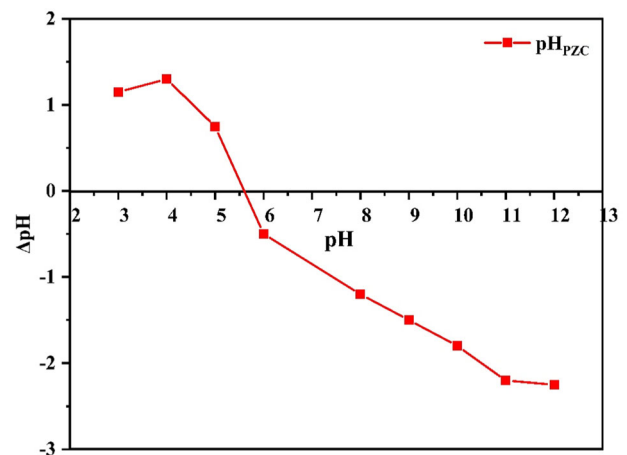


Fig. 10 Point of zero charge of HCAC4

with an agitation speed of 150 rpm. A 30-min difference was made in the contact time, which ranged from 30 to 90 min. At a contact duration of 60 min, the major elimination of 96.63% was achieved.

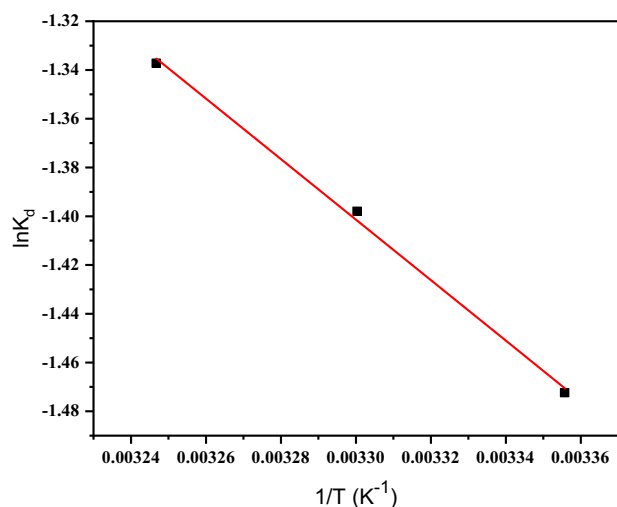


Fig. 11 Van't Hoff plot of Fe^{2+} adsorption on the prepared activated carbon

3.5 Thermodynamic parameters

The process's thermodynamic characteristics, including the change in free energy (ΔG°), change in enthalpy (ΔH°) and change in entropy (ΔS°) were determined using the following formulas [19]. Fig 11 shows the van't Hoff plot for adsorption of Fe^{3+} on the prepared activated carbon.

$$K_c = \frac{q_e}{C_e}$$

$$\Delta G^\circ = -RT \ln K_c \quad (13)$$

$$\ln K_c = \frac{\Delta S^\circ}{R} - \frac{\Delta H^\circ}{RT}$$

where K_c denotes the equilibrium constant, C_e is the equilibrium concentration in solution (mg/L), and q_e is the concentration in the solid phase at equilibrium (mg/L). The $\ln K_c$ against $1/T$ linear Van't Hoff plot's slope and intercept were used to calculate the corresponding ΔH° and ΔS° values. The determined values of the thermodynamic parameters for the adsorption of Fe^{3+} on activated carbon are displayed in Table 8. The feasibility and spontaneous thermodynamic adsorption of Fe^{3+} on activated carbon based on horse chestnut shell were demonstrated at all temperatures using negative values of ΔG° . When Fe^{3+} is adsorbed on activated carbon, there is enhanced randomness at the solid-solution interface and an exothermic adsorption interaction, as indicated by the negative value of ΔH° . The adsorption energy is very high as the system tends to release energy and there is a strong chemical binding between adsorbate and adsorbent surface. This also leads to the surface reactions and change in surface properties. There are now more potential microstates than before. The process of adsorption is chemical.

Table 8 Thermodynamic parameters of the adsorption of Fe^{3+}

T (K)	ΔG° (Kj/mol)	ΔH° (Kj/mol)	ΔS° (Kj/mol K)
283	-16.98	-103.16	22.38
288	-16.76		
293	-16.87		
298	-16.98		
303	-17.1		
308	-17.21		

3.6 Adsorption mechanism

Physical adsorption, chemisorption, ion exchange, and pore diffusion mechanisms are all involved in the adsorption of Fe^{3+} ions onto activated carbon made from horse chestnut shell. Because of its vast microporosity and high surface area resulting from KOH activation, activated carbon offers a multitude of sites for physical adsorption via van der Waals forces and electrostatic interactions. Additionally important is chemisorption, wherein functional groups on the carbon surface such as hydroxyl, carboxyl, and carbonyl groups form strong coordination interactions with Fe^{3+} ions to enhance adsorption effectiveness, especially at particular pH levels. Furthermore, as Fe^{3+} ions take the place of exchangeable cations like H^+ or K^+ on the activated carbon surface, ion exchange takes place. This process is corroborated by pH variations that are seen during adsorption. Fe^{3+} ions diffuse into the pores of carbon, which amplifies the adsorption process. The intraparticle diffusion model suggests that diffusion rates affect the total amount of adsorption. Thermodynamic analysis demonstrates that the adsorption is exothermic and spontaneous, and its enhanced favourability at lower temperatures is confirmed by negative Gibbs free energy values. The high adsorption capacity found can be attributed to a number of mechanisms, including the presence of functional groups and optimised pore structure. These findings provide important insights into the design of activated carbon that can be used to remove heavy metals from aqueous solutions.

4 Conclusion

The activated carbons used in this investigation were made from horse chestnut shells, a rarely used raw material for preparation of activated carbon by potassium hydroxide (KOH) activation. It was established that the activated carbon's maximum specific surface area and total pore volume were $685.808 \text{ m}^2/\text{g}$ and 0.22 cc/g , respectively. TGA, SEM, BET, EDX, FTIR, and XRD techniques were used to characterize the raw material and the activated carbons that were produced. The highest surface area

activated carbon (685.808 m²/g) that was generated was utilized to extract Fe³⁺ from aqueous solutions. The equilibrium, kinetics and thermodynamics aspects of the adsorption were evaluated, the study implied that the pseudo-second-order equation provided the better correlation of the adsorption data. Also, Langmuir model was found to provide the best fit of the experimental data and maximum adsorption capacity was found equal to 138.88 mg/g at pH 6. Based on the obtained results it appears that the activated carbon prepared from horse chestnut shell constitutes a great adsorbent property for removing Fe³⁺ ions from aqueous system for environmental protection purpose.

Acknowledgements The authors extend their appreciation to the Division of Research Centre for Residue and Quality Analysis at Sher-e-Kashmir University of Agriculture Science and Technology, Kashmir, for providing access to the Atomic absorption spectrophotometer and facilitating its use in this study.

Author contributions Uzma Imtiaz wrote, formatted, structured the manuscript. Performed the experiments, analysis and curated the data. Mushtaq AH. Rather supervised and conceptualized the manuscript.

Compliance with ethical standards

Conflict of interest The authors declare no competing interests.

Abbreviation

AAS	Atomic Absorption Spectroscopy
ASTM	American Standards of Testing Material
HCAC	Horse chestnut activated carbon
KOH	Potassium Hydroxide
FTIR	Fourier Transform Infra-Red
SEM	Scanning Electron Microscope
EDX	Energy Dispersive X-ray Spectroscopy
XRD	X-Ray Diffraction
DR	Dubinon Radushkevich
TGA	Thermo-gravimetric Analysis

References

- Edo GI, Samuel PO, Oloni GO, Ezekiel GO, Ipekoru VO, Obasohan P, Ongulu J, Otunuya CF, Opiti AR, Ajakaye RS, Essaghah AEA, Agbo JJ (2024) Environmental persistence, bioaccumulation, and ecotoxicology of heavy metals. *Chem. Ecol.* 40:322–349. <https://doi.org/10.1080/02757540.2024.2306839>
- Sharma A, Grewal AS, Sharma D, Srivastav AL (2023) Heavy metal contamination in water: consequences on human health and environment, in: *Metals in Water*. Elsevier, pp. 39–52. <https://doi.org/10.1016/b978-0-323-95919-3.00015-x>
- Baksh P, Jugade R (2023) Phytostabilization and rhizofiltration of toxic heavy metals by heavy metal accumulator plants for sustainable management of contaminated industrial sites: A comprehensive review. *J. Hazard. Mater. Adv.* <https://doi.org/10.1016/j.hazadv.2023.100293>
- Sable H, Singh V, Kumar V, Roy A, Pandit S, Kaur K, Rustagi S, Malik S (2024) Toxicological and bioremediation profiling of nonessential heavy metals (mercury, chromium, cadmium, aluminium) and their impact on human health: A review. *Toxicol. Anal. Clin.* <https://doi.org/10.1016/j.toxac.2024.03.096>
- World Health Organization, (2022) Guidelines for drinking-water quality: fourth edition incorporating the first and second addenda. World Health Organisation 1–583
- Bis, I. (2012) 10500 Indian standard drinking water–specification, second revision. Bureau of Indian Standards, New Delhi
- Sun Y, Chen F, Zafar A, Khan ZI, Ahmad K, Ch SA, Batool AI, Nadeem M (2023) Assessment of potential toxicological risk for public health of heavy metal iron in diverse wheat varieties irrigated with various types of waste water in South Asian country. *Agric. Water Manag.* 276:108044. <https://doi.org/10.1016/j.agwat.2022.108044>
- Hama Aziz KH, Mustafa FS, Omer KM, Hama S, Hamarawf RF, Rahman KO (2023) Heavy metal pollution in the aquatic environment: efficient and low-cost removal approaches to eliminate their toxicity: a review. *RSC Adv* 13:17595–17610. <https://doi.org/10.1039/d3ra00723e>
- Kolya H, Kang CW (2023) Next-generation water treatment: exploring the potential of biopolymer-based nanocomposites in adsorption and membrane filtration. *Polymers (Basel)* 15:3421. <https://doi.org/10.3390/polym15163421>
- Al-Gethami W, Qamar MA, Shariq M, Alaghaz ANMA, Farhan A, Areshi AA, Alnasir MH (2024) Emerging environmentally friendly bio-based nanocomposites for the efficient removal of dyes and micropollutants from wastewater by adsorption: a comprehensive review. *RSC Adv* 14:2804–2834. <https://doi.org/10.1039/d3ra06501d>
- Ramalingam G, Priya AK, Gnanasekaran L, Rajendran S, Hoang TKA (2024) Biomass and waste derived silica, activated carbon and ammonia-based materials for energy-related applications – A review. *Fuel* 355:129490. <https://doi.org/10.1016/j.fuel.2023.129490>
- Selene O, Peano C, Sottile F (2024) Recent Innovations on the Reuse of Almond and Hazelnut By-Products: A Review. *Sustainability* 16:2577
- Packialakshmi S, Anuradha B, Nagamani K, Sarala Devi J, Sujatha S (2021) Treatment of industrial wastewater using coconut shell based activated carbon. *Mater. Today Proc.* 81:1167–1171. <https://doi.org/10.1016/j.matpr.2021.04.548>
- Kyei SK, Eke WI, Nagre RD, Mensah I, Akaranta O (2023) A comprehensive review on waste valorization of cashew nutshell liquid: Sustainable development and industrial applications. *Clean. Waste Syst.* 6:100116. <https://doi.org/10.1016/j.clwas.2023.100116>
- Sibagariang YP, Napitupulu FH, Kawai H, Ambarita H (2023) Study on the effect of oil palm shells on fresh water productivity of double slope solar still. *J. Energy Storage* 70:108000. <https://doi.org/10.1016/j.est.2023.108000>
- Ollani S, Peano C, Sottile F (2024) Recent innovations on the reuse of almond and hazelnut by-products: a review. *Sustain* 16:2577. <https://doi.org/10.3390/su16062577>
- Brishti RS, Kundu R, Habib MA, Ara MH (2023) Adsorption of iron(III) from aqueous solution onto activated carbon of a natural source: Bombax ceiba fruit shell. *Results Chem* 5:100727. <https://doi.org/10.1016/j.rechem.2022.100727>
- Lin Y, Alengaram UJ, Ibrahim Z (2023) Effect of treated and untreated rice husk ash, palm oil fuel ash, and sugarcane bagasse ash on the mechanical, durability, and microstructure characteristics of blended concrete – A comprehensive review. *J. Build. Eng.* 78:107500. <https://doi.org/10.1016/j.jobee.2023.107500>
- Yang K, Wang X, Wu H, Fang N, Liu Y, Zhang C, Yu X, Wang X (2023) Adsorption of pyraclostrobin in water by bamboo-

- derived and pecan shell-derived biochars. *Sustain* 15:14585. <https://doi.org/10.3390/su151914585>
20. Akkari I, Graba Z, Bezzi N, Kaci MM, Merzeg FA, Bait N, Ferhati A, Dotto GL, Benguerba Y (2023) Effective removal of cationic dye on activated carbon made from cactus fruit peels: a combined experimental and theoretical study. *Environ. Sci. Pollut. Res.* 30:3027–3044. <https://doi.org/10.1007/s11356-022-22402-4>
 21. Akkari I, Graba Z, Bezzi N, Vithanage M, Kaci MM (2022) New insights into the effective removal of Basic Red 46 onto activated carbon produced from pomegranate peels. *Biomass Convers. Biorefinery*. <https://doi.org/10.1007/s13399-022-03401-4>
 22. Stachowicz P, Stolarski MJ (2023) Short rotation woody crops and forest biomass sawdust mixture pellet quality. *Ind. Crops Prod.* 197:116604. <https://doi.org/10.1016/j.indcrop.2023.116604>
 23. Şenol ZM, El Messaoudi N, Fernine Y, Keskin ZS (2024) Bioremoval of rhodamine B dye from aqueous solution by using agricultural solid waste (almond shell): experimental and DFT modeling studies. *Biomass Convers. Biorefinery* 14:17927–17940. <https://doi.org/10.1007/s13399-023-03781-1>
 24. Alardhi SM, Salih HG, Ali NS, Khalbas AH, Salih IK, Saady NMC, Zendejboudi S, Albayati TM, Harharah HN (2023) Olive stone as an eco-friendly bio-adsorbent for elimination of methylene blue dye from industrial wastewater. *Sci. Rep.* 13:21063. <https://doi.org/10.1038/s41598-023-47319-x>
 25. Sosa JA, Laines JR, García DS, Hernández R, Zappi M, Espinosa de los Monteros, AE (2023) Activated carbon: A review of residual precursors, synthesis processes, characterization techniques, and applications in the improvement of biogas. *Environ. Eng. Res.* 28. <https://doi.org/10.4491/eer.2022.100>
 26. Turkyilmaz A, Isinkaralar K, Dogan M, Kocer Kizilduman B, Bicil Z (2024) Production, characterization, and hydrogen storage properties of activated carbon from horse chestnut shell. *Sustain. Chem. Pharm.* 40:101634. <https://doi.org/10.1016/j.scp.2024.101634>
 27. Konduri VV, Kalagatur NK, Gunti L, Mangamuri UK, Kalagadda VR, Poda S, Krishna SBN (2024) Green synthesis of silver nanoparticles from *Hibiscus tiliaceus* L. Leaves and their applications in dye degradation, antioxidant, antimicrobial, and anticancer activities. *South African J. Bot.* 168:476–487. <https://doi.org/10.1016/j.sajb.2024.03.035>
 28. Teymur YA, Güzel F, İnal IG (2023) High surface area mesoporous carbon from black cumin (*Nigella sativa*) processing industry solid residues via single-stage K₂CO₃ assisted carbonization method: Production optimization, characterization and its some water pollutants removal and supercapacitor performance. *Diam. Relat. Mater.* 135:109815. <https://doi.org/10.1016/j.diamond.2023.109815>
 29. Isinkaralar K, Gullu G, Turkyilmaz A (2023) Experimental study of formaldehyde and BTEX adsorption onto activated carbon from lignocellulosic biomass. *Biomass Convers. Biorefinery* 13:4279–4289. <https://doi.org/10.1007/s13399-021-02287-y>
 30. Durak H, Genel S (2024) Investigation of the effect of metal powder and metal-supported MCM-41 catalysts on the pyrolysis of horse chestnut fruits and shells (*Aesculus hippocastanum* L.). *Biomass Convers. Biorefinery* 1–12. <https://doi.org/10.1007/s13399-024-05772-2>
 31. Izquierdo S, Pacheco N, Durán-Valle CJ, López-Coca IM (2023) From waste to resource: utilizing sweet chestnut waste to produce hydrothermal carbon for water decontamination. *C-Journal Carbon Res* 9:57. <https://doi.org/10.3390/c9020057>
 32. Zaman F, Ishaq MW, Munawar A, Younas U, Ali Z (2023) *Aesculus indica*-derived heteroatom-doped carbon as an electrode material for super-capacitor. *Carbon Lett* 33:1967–1976. <https://doi.org/10.1007/s42823-023-00565-5>
 33. Amen R, Yaseen M, Mukhtar A, Klemeš JJ, Saqib S, Ullah S, Al-Sehemi AG, Rafiq S, Babar M, Fatt CL, Ibrahim M, Asif S, Qureshi KS, Akbar MM, Bokhari A (2020) Lead and cadmium removal from wastewater using eco-friendly biochar adsorbent derived from rice husk, wheat straw, and corncob. *Clean. Eng. Technol.* 1:100006. <https://doi.org/10.1016/j.clet.2020.100006>
 34. Kaveeshwar AR, Ponnusamy SK, Revellame ED, Gang DD, Zappi ME, Subramaniam R (2018) Pecan shell based activated carbon for removal of iron(II) from fracking wastewater: Adsorption kinetics, isotherm and thermodynamic studies. *Process Saf. Environ. Prot.* 114:107–122. <https://doi.org/10.1016/j.psep.2017.12.007>
 35. Palma C, Lloret L, Puen A, Tobar M, Contreras E (2016) Production of carbonaceous material from avocado peel for its application as alternative adsorbent for dyes removal. *Chinese J. Chem. Eng.* 24:521–528. <https://doi.org/10.1016/j.cjche.2015.11.029>
 36. Aboua KN, Yobouet YA, Yao KB, Goné DL, Trokourey A (2015) Investigation of dye adsorption onto activated carbon from the shells of Macoré fruit. *J. Environ. Manage.* 156:10–14. <https://doi.org/10.1016/j.jenvman.2015.03.006>
 37. Brudey T, Largitte L, Jean-Marius C, Tant T, Dumesnil PC, Lode-wyckx P (2016) Adsorption of lead by chemically activated carbons from three lignocellulosic precursors. *J. Anal. Appl. Pyrolysis* 120:450–463. <https://doi.org/10.1016/j.jaap.2016.06.018>
 38. Uddin MK, Nasar A (2020a) Walnut shell powder as a low-cost adsorbent for methylene blue dye: isotherm, kinetics, thermodynamic, desorption and response surface methodology examinations. *Sci. Rep.* 10:7983. <https://doi.org/10.1038/s41598-020-64745-3>
 39. Nassef HM, Al-Hazmi GAAM, Alayyafi AAA, El-Desouky MG, El-Bindary AA (2024) Synthesis and characterization of new composite sponge combining of metal-organic framework and chitosan for the elimination of Pb(II), Cu(II) and Cd(II) ions from aqueous solutions: Batch adsorption and optimization using Box-Behnken design. *J. Mol. Liq.* 394:123741. <https://doi.org/10.1016/j.molliq.2023.123741>
 40. Uddin MK, Nasar A (2020b) Decolorization of basic dyes solution by utilizing fruit seed powder. *KSCE J. Civ. Eng.* 24:345–355. <https://doi.org/10.1007/s12205-020-0523-2>
 41. Gayathiri M, Pulingam T, Lee KT, Mohd Din AT, Kosugi A, Sudesh K (2023) Sustainable oil palm trunk fibre based activated carbon for the adsorption of methylene blue. *Sci. Rep.* 13:429–437. <https://doi.org/10.1038/s41598-023-49079-0>
 42. Alabi-Babalola O, Aransiola E, Asuquo E, Garforth A, D'Agostino C (2024) Production of Highly Efficient Activated carbons for Wastewater Treatment from Post-Consumer PET Plastic Bottle Waste. *Chempluschem* 89:202300484. <https://doi.org/10.1002/cplu.202300484>
 43. Romero-Hernandez JJ, Paredes-Laverde M, Silva-Agredo J, Mercado DF, Ávila-Torres Y, Torres-Palma RA (2024) Pharmaceutical adsorption on NaOH-treated rice husk-based activated carbons: Kinetics, thermodynamics, and mechanisms. *J. Clean. Prod.* 434:139935. <https://doi.org/10.1016/j.jclepro.2023.139935>
 44. Bednárek J, Matějová L, Koutník I, Vráblová M, Cruz GJF, Strašák T, Šiler P, Hrbáč J (2024) Revelation of high-adsorption-performance activated carbon for removal of fluoroquinolone antibiotics from water. *Biomass Convers. Biorefinery* 14:2585–2599. <https://doi.org/10.1007/s13399-022-02577-z>
 45. Mve Mfoumou C, Tonda-Mikiéla P, Ngoye F, Bouassa Mounala S, Mbouiti BL, Feuya Tchouya GR (2024) Removal and adsorption kinetics of copper(II) ions from aqueous media on activated carbon in dynamic adsorption on a fixed-bed column. *Comptes Rendus. Chim.* 27:141–151. <https://doi.org/10.5802/crchim.285>
 46. Wu H, Chen R, Du H, Zhang J, Shi L, Qin Y, Yue L, Wang J (2019) Synthesis of activated carbon from peanut shell as dye adsorbents for wastewater treatment. *Adsorpt. Sci. Technol.* 37:34–48. <https://doi.org/10.1177/0263617418807856>

47. Youssef WM, El-Maadawy MM, Masoud AM, Alhindawy IG, Hussein AEM (2024) Uranium capture from aqueous solution using palm-waste based activated carbon: sorption kinetics and equilibrium. *Environ. Monit. Assess.* 196:428. <https://doi.org/10.1007/s10661-024-12560-y>
48. Musah M, Yisa J, Suleiman MT, Abdullahi M, Shaba EY (2018) Study of isotherm models for the adsorption of Cr(VI) ion from aqueous solution onto Bombax buonopozense calyx activated carbon. *Lapai J. Sci. Technol* 4:22–32
49. Yakubu MK, Abdullahi AM (2008) Use of activated carbon from date seeds to treat textile and tannery effluents. *African J. Sci. Technol. Sci. Eng. Ser.* 9:39–49
50. Dada AO, Inyinbor AA, Tokula BE, Bayode AA, Obayomi KS, Ajanaku CO, Adekola FA, Ajanaku KO, Pal U (2024) Zinc oxide decorated plantain peel activated carbon for adsorption of cationic malachite green dye: Mechanistic, kinetics and thermodynamics modeling. *Environ. Res.* 252:119046. <https://doi.org/10.1016/j.envres.2024.119046>
51. Wang B, Lan J, Bo C, Gong B, Ou J (2023) Adsorption of heavy metal onto biomass-derived activated carbon: review. *RSC Adv* 13:4275–4302. <https://doi.org/10.1039/d2ra07911a>
52. Nimibofa A, Tobin EA, David SN, Donbebe W, Dixon DE (2017) Ravnotežna, kinetička i termodinamička studija izdvajanja bakra pomoću slojevitog dvostrukog hidroksida. *Hem. Ind.* 71:429–437. <https://doi.org/10.2298/HEMIND150608005N>
53. Uteeva ZD, Sadykov RU, Bagdanova DO, Agliullin MR, Guskov VY (2024) Adsorption isotherms of enantiomers on a chiral open-framework copper borophosphate $\text{LiCu}_2[\text{BP}_2\text{O}_8(\text{OH})_2]$. *New J. Chem.* 48:7189–7196. <https://doi.org/10.1039/d4nj00314d>
54. Sema AI, Bhattacharyya J (2022) Biochar derived from waste bamboo shoots for the biosorptive removal of ferrous ions from aqueous solution. *J. Indian Chem. Soc.* 99:100791. <https://doi.org/10.1016/j.jics.2022.100791>
55. Kamboj V, Tiwari DP (2024) Removal of heavy metal (Cu, Cr, and Ni) ions from aqueous solution using derived activated carbon from water hyacinth. *Biomass Convers. Biorefinery* 14:5075–5083. <https://doi.org/10.1007/s13399-022-02702-y>
56. Demiral İ, Samdan C, Demiral H (2021) Enrichment of the surface functional groups of activated carbon by modification method. *Surfaces and Interfaces* 22:100873. <https://doi.org/10.1016/j.surfin.2020.100873>
57. Heidarinejad Z, Dehghani MH, Heidari M, Javedan G, Ali I, Sillanpää M (2020) Methods for preparation and activation of activated carbon: a review. *Environ. Chem. Lett.* 18:393–415. <https://doi.org/10.1007/s10311-019-00955-0>

Publisher's note Springer Nature remains neutral with regard to jurisdictional claims in published maps and institutional affiliations.

Springer Nature or its licensor (e.g. a society or other partner) holds exclusive rights to this article under a publishing agreement with the author(s) or other rightsholder(s); author self-archiving of the accepted manuscript version of this article is solely governed by the terms of such publishing agreement and applicable law.